Assessing temporal variability and controlling factors of the sediment budget of a small agricultural catchment in Northern France (the Pommeroye)

Edouard Patault, Claire Alary, Christine Franke, Arnaud Gauthier, Nor-Edine Abriak

Assessing temporal variability and controlling factors of the sediment budget of a small agricultural catchment in Northern France (the Pommeroye).

Edouard Patault[a,b,c], Claire Alary[a], Christine Franke[b], Arnaud Gauthier[d], Nor-Edine Abriak[a]

[a]*IMT Lille Douai, Univ. Lille, EA 4515 – LGgE – Civil Engineering and Environmental Department, F-59000 Lille, France*

[b]*MINES ParisTech, PSL Research University, Center of Geosciences, 35 rue Saint-Honoré, 77305 Fontainebleau Cedex, France*

[c]*Normandie Univ, Rouen, UNIROUEN, UNICAEN, CNRS, M2C, FED-SCALE, Rouen, France*

[d]*Département des Sciences de la Terre, Université de Lille 1, Villeneuve d'Ascq, France*

Corresponding author: edouard.patault1@univ-rouen.fr ; Phone: (+33)6.25.99.17.08

Abstract

A high-frequency monitoring station was implemented at the outlet of the small catchment of the Pommeroye (0.54 km²) in Northern France to study erosion by runoff and hydro-sedimentological responses to heavy rainfall events in the context of Quaternary loess deposits. The aim of this experimental work is to assess the temporal variability of sediment yield and to identify the factors controlling the hydro-sedimentary response. To achieve this goal, statistical and hydro-sedimentary dynamic analyses were performed. During two years of monitoring (April 2016 – April 2018), 48 flood events were recorded. The specific sediment yield (SSY) is highly variable and was evaluated to 29.4-70 t km^{-2} yr^{-1} which is conventional for the study region. Most of the sediment yield was produced in winter (55%) and autumn (42%). Only 3% of SSY were produced during spring and summer periods. According to our results, only 6% of the erosive events are responsible for the

transport of more than 40% of the sediment flux recorded at the outlet. This underlines the temporal variability of the hydro-sedimentary production in small agricultural catchments for which most of the hydro-sedimentary flux is produced during a limited number of events. The results of statistical analyses show that the total amount of rainfall and the duration of a rainfall episode are the main controlling factors on the hydro-sedimentary response. Our results also suggest that the rainfall kinetic energy better reflects the sediment detachment, and that the 48 h-antecedent rainfall is not linked to the hydro-sedimentary response.

1 Introduction

In the North-Western European loess plateau and in particular in the North of the Paris Basin, erosion of agricultural land is a serious environmental issue (Evrard et al., 2007; Delmas et al., 2012). Every year, numerous natural disasters occur due to various erosion processes which result in on-site and off-site problems including the loss of fertile soils, the silting of riverbeds and dams, as well as infrastructure and property damage by muddy floods (Capra, 1993). The most common type of soil erosion pattern observed in these territories are (i) sheet erosion, (ii) rills, (iii) interrills, (iv) classical gullies, and (v) ephemeral gullies (Foster, 1986). So far, the focus was drawn to rill/interrill erosion, but recently a growing interest has focused on ephemeral gullies (Poesen, 1993; Nachtergaele et al., 2002; Valentin et al., 2005; Castillo and Gomez, 2016), since they have been recognized as a major contributor to sediment yield in small agricultural catchments in the European loess belt (Poesen et al., 1996). Classical survey methods to evaluate sediment production on small catchments are aerial photography (Nachtergaele and Poesen, 1999; Marzolff et al., 2011), terrestrial photography (Frankl et al., 2011), terrestrial laser scanning (Li et al., 2017), airborne laser scanning (Goodwin et al., 2017), or direct measurements of channel volumes (Valcárcel et al., 2003). However, these methodologies are not suitable for quantifying the sediment yield at the catchment scale (Vandaele and Poesen, 1995). Understanding and quantifying the dynamics of suspended sediment transport is essential for controlling soil erosion and implementing effective mitigation practices to reduce stream suspended matter and associated pollutants discharge. Currently, catchment monitoring was successfully used

by several authors (Nadal-Romero et al., 2008; Estrany et al., 2009; Nu-Fang et al., 2011; Giménez et al., 2012; Sherriff et al., 2015) to quantify erosion processes in agricultural catchments and to assess the relationships between hydro-sedimentological parameters. These studies have reported on sediment transfer that show high temporal and spatial variabilities, and the fact that only few erosive events are responsible for the majority of the sediment export (Gay et al., 2014; Bagarello et al., 2017; Grangeon et al., 2017). They also report on complex correlations between rainfall characteristics and the hydro-sedimentary response. Some attempts have been made to evaluate the variability of the hydro-sedimentary response at larger scale in the context of agricultural plains of North-Western Europe (Cerdan et al., 2010; Vanmaercke et al., 2011), but according to Poesen (2018), very few studies have measured the water erosion dynamic on relatively small catchments (0.01 - 1000ha). At this scale range, there is a shift in the dominance of particular erosion processes. As reported by Vanmaercke et al. (2011), small headwater lowland catchments may exhibit significant sediment export. According to Grangeon et al. (2017), the spatial and temporal dynamics of sediment fluxes must be further studied to improve our understanding of the possible connection/disconnection between the water and the sediment transport pathways, in particular for areas where intensive agriculture is predominant and runoff can be generated by soil saturation (Gay et al., 2016). Some recent studies already point out that connectivity between sediment sources and rivers is essential for soil redistribution (Landemaine et al., 2015; Foucher et al., 2015; Heckmann et al., 2018). Sediment flux data for such small catchments are therefore essential for better understanding the linkages between soil erosion processes and suspended sediment transport of larger rivers (Verstraeten and Poesen, 2001). However, quantification of the sediment yield at this scale might be challenging, especially if there is a lack of a perennial hydrographic network in the studied catchment.

Generally, the characterization and quantification of sedimentary flow is limited to experimental data of spot samples at the outlet of the watershed and therefore does not necessarily take into account the internal dynamics of the basin (Foucher, 2015).

In the context of the Canche River watershed (Northern France), erosion of agricultural lands may lead to particularly devastating muddy flows that generate an important export of sediments and a high material costs for the local communities. Since 1983, 1100 municipalities were stroke by heavy muddy flows. So far, any systematic study was conducted to better understand the genesis of these phenomena. Thus, the local Water Agency expressed the clear need for high-resolution data on the Canche River watershed, to be able to quantify the sediment exported by mudflows, to define their respective temporal variability, and to identify the main controlling factors.

Nevertheless, the understanding of the hydro-sedimentary fluxes variability and the associated factors on the Canche River watershed first requires the monitoring and understanding of processes at the scale of the experimental catchment. The goal of this study was to deploy a high-frequency monitoring station in a challenging context since the small studied catchment (0.54 km²) is lacking a perennial hydrographic network. The hydro-sedimentary behavior was characterized with a high-temporal resolution (6 min). To this end, runoff events are monitored over two hydrological years (April 2016 to April 2018). This allows to: (i) quantify short-term changes between different runoff events, (ii) identify the main controlling factors, and (iii) determine the temporal variability. These results are crucial to be able to better address the existing soil erosion problems in northern France related to rain events runoff.

2 Study area

The Pommeroye catchment (0.54 km²) is situated in the European loess belt in Northern France (Fig. 1A). It is a sub-catchment of the Canche River watershed (1274 km²). The dominant climate is oceanic and the average annual temperature in this region is 11°C. The thermal amplitude is low, with soft winters and cool summers. The annual rainfall amount is 1000 ± 150 mm yr^{-1}. An ephemeral gully network is well-established and recurrent, resulting from the junction of rills that form a dendritic channel pattern (Fig. 1B). The elevation of the study area ranges from 115 to 145 m and the average slope is 4.2% (Fig. 1C). The soil is constituted of Pleistocene silt which overlays the

chalky soil of the Seno-Turonian (Beckelynck, 1981). Grain size analyzes carried out by Patault (2018), on 22 agricultural soil samples, in the Canche watershed, show that agricultural soils are composed of clay (5%), silts (54%), and fine sands (41%). The medium-textured soils (loamy soils) tend to be most erodible because they have high amounts of silts and very fine sand. These soils tend to have the highest soil erodibility factor in Europe (K > 0.055 t ha h ha^{-1} MJ^{-1} mm^{-1}; Panagos et al., 2014). The study site is exclusively occupied by arable land, divided into 14 fields. The dominant crops here are cereals, winter and spring barley, rape seed, and mustard.

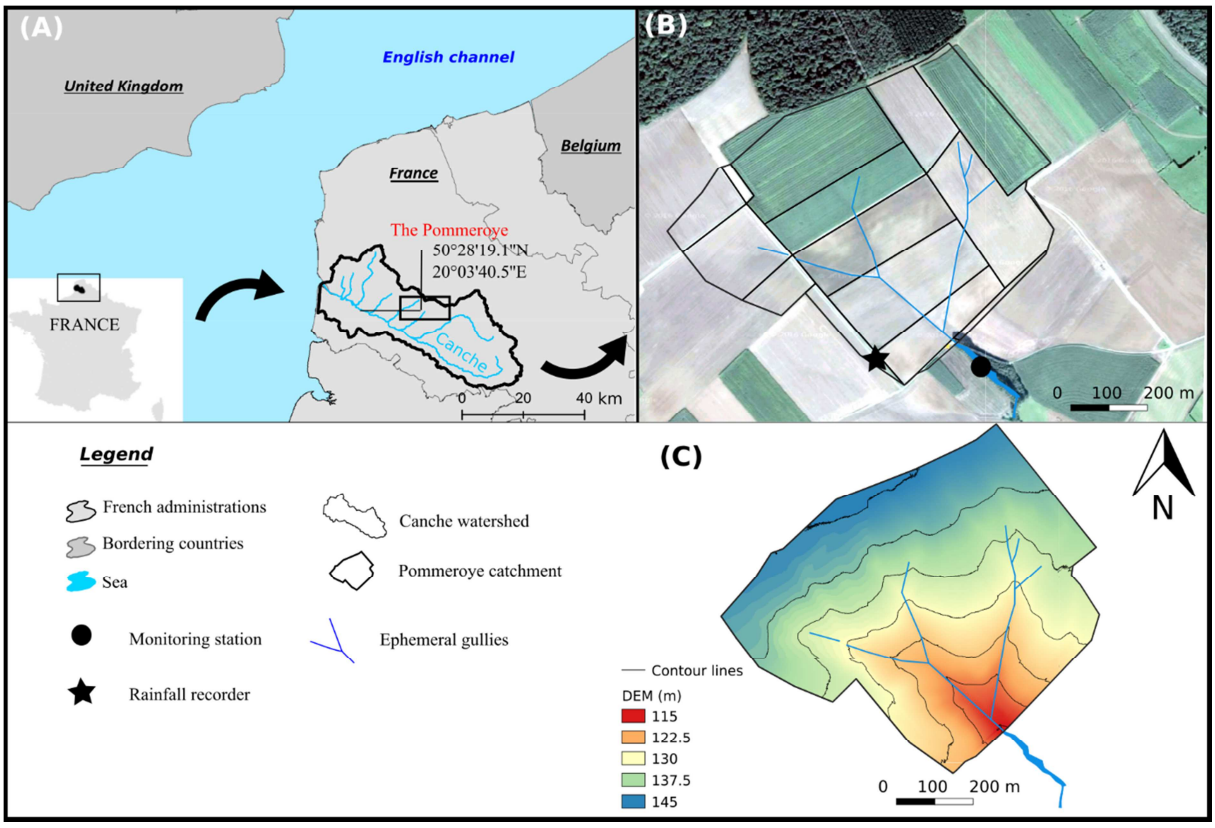

Fig. 1: (A) Overview on the study region, (B) map of the Pommeroye catchment showing the location of the ephemeral gullies and instruments used in this study, (C) Digital Elevation Model (DEM) of the study site (cell size: 50 cm).

3 Material & Methods

3.1 The monitoring station

A monitoring station consisting of an exponential Venturi channel and an approach channel has been installed on March 31, 2016 at the outlet of the Pommeroye catchment to record the flow

discharge and suspended sediment concentration (SSC). The hypothetic maximum flow discharge was estimated using the rational equation for peak discharge (Thompson, 2006). The rational method is a simple technique for estimating a design discharge from a small catchment. The method is based on the simple equation that relates the runoff-producing potential of the catchment, the average intensity of rainfall for a particular length of time (the time of concentration), and the catchment area (Eq.1):

$$Q = C \times i \times A \quad (1)$$

Where Q is the design discharge ($m^3\ s^{-1}$), C is the runoff coefficient (between 0 and 1; a value of 0.1 is usually applied for agricultural lands), i is the design rainfall intensity (mm h^{-1}), and A is the catchment drainage area (ha). The design rainfall intensity is defined using the Montana coefficients (Eq.2):

$$i = a \times t^{-b} \quad (2)$$

Where t is the concentration time (t = 0.34 h), a and b are the Montana coefficients at the closest meteorological station. Here, the closest station for which the coefficient are available was the station of Le Touquet-Paris-Plage (a = 23.3 and b = 0.67). Using the rational method, the design discharge was evaluated to 0.72 $m^3\ s^{-1}$, which is slightly over-evaluated considering that the station of Le Touquet-Paris-Plage is located in an area that is affected by slightly higher rainfall than the study area. The Venturi channel VII provided by ISMA allowed a maximum discharge of 0.40 $m^3\ s^{-1}$, which was considered in adequacy with the objectives of our study.

According to the calculated maximum flow discharge, a Venturi channel (*Venturi channel ISMA VII*) of suitable dimensions for measuring the hypothetic discharge has been selected (Fig.2). The length of the approach channel was established considering the *ISO 4359 standard* (AFNOR, 1986) that requires an approach length of at least 5 times the width of the channel approach,

upstream of the load measurement zone. This corresponds to three to four times the maximum height to be measured, upstream of the Venturi's contraction. The approach channel assures the passage of the torrential flow generated by the various constraints of ground, to a river regime at the entrance of the Venturi channel, necessary for the validity of an adapted monitoring. The Venturi and the approach channel are positioned horizontally, without any slope, in the longitudinal and transversal direction. They are perfectly aligned and are thus not affected by any profile changes. An ultrasound water-level logger (*Ijinus LNU 300-X*) records the water height in the Venturi channel.

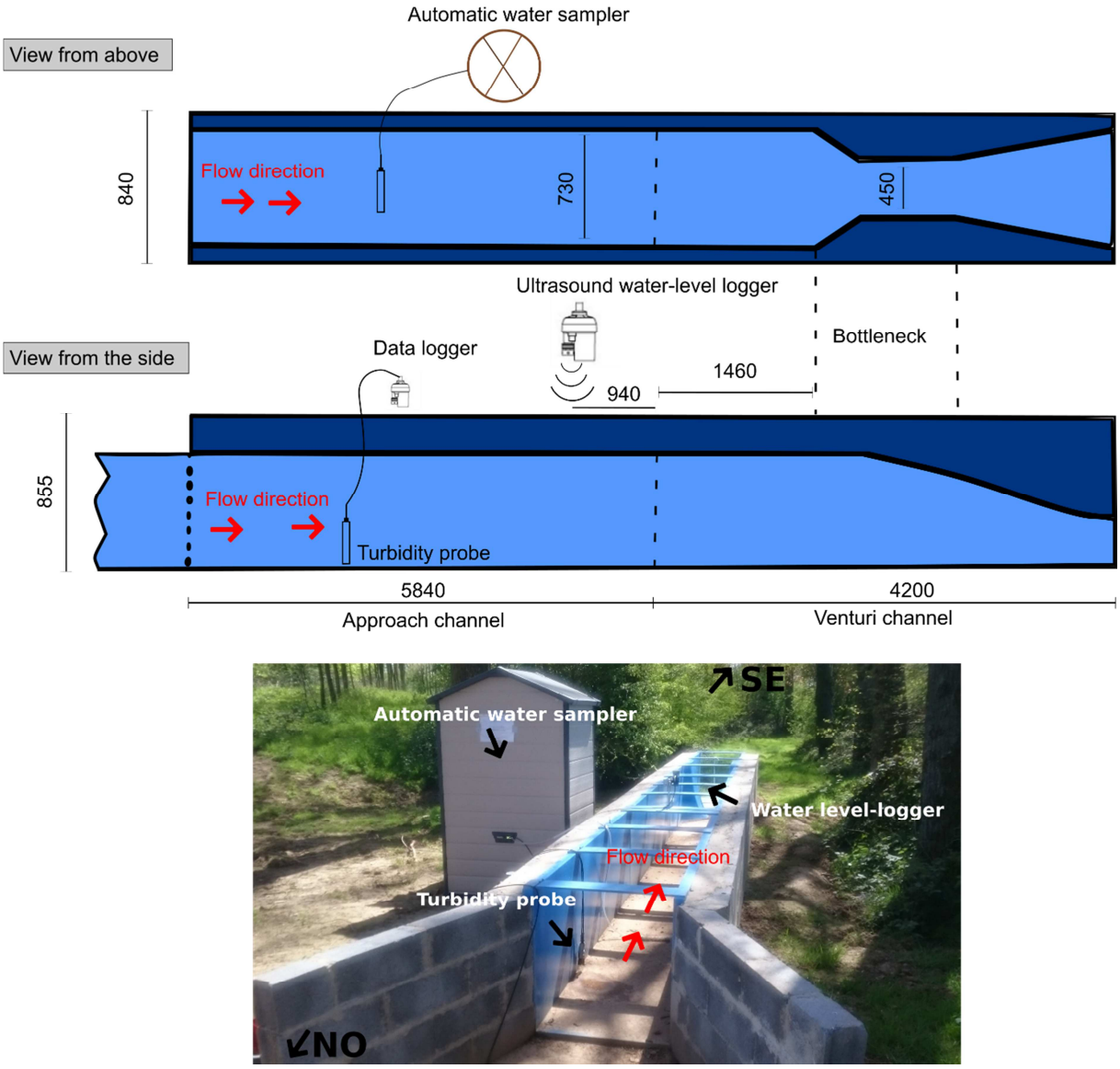

Fig. 2: Schema and picture of the monitoring station at the outlet of the Pommeroye catchment viewed from different perspectives (the dimensions are given in mm).

106 Runoff discharge is calculated for each time step in the Venturi channel using the following
107 equation (Eq.3) and a conversion table (Table 1) provided by the manufacturer (*ISMA*; *www.isma.fr*)
108 of the Venturi channel. The relation between height and flow discharge was defined by the
109 manufacturer and validated using in-situ experimentation and 3-D modelling (Dufresne et al., 2010):

$$Q = -7{,}223 \times h + 2873{,}2 \times h^2 - 766 \times h^3 + 770 \times h^4 \quad (3)$$

110

111 Where Q is the flow discharge in the Venturi channel ($m^3\ h^{-1}$) and h the water height (m).

Table 1 : Conversion table of height (mm) and flow discharge ($m^3\ h^{-1}$) for the Venturi channel *ISMA VII*, provided by the manufacturer.

h (mm)	Q ($m^3\ h^{-1}$)	h (mm)	Q ($m^3\ h^{-1}$)
73	14.51	410	448.99
80	17.45	425	482.22
95	24.65	440	516.68
110	33.06	455	552.39
125	42.68	470	589.34
140	53.50	485	627.56
155	65.50	500	667.06
170	78.69	515	707.86
185	93.05	530	749.97
200	108.59	545	793.41
215	125.29	560	838.19
230	143.17	575	884.35
245	162.20	590	931.88
260	182.41	605	980.83
275	203.77	620	1031.20
290	226.31	635	1083.02
305	250.01	650	1136.32
320	274.88	665	1191.12
335	300.92	680	1247.44
350	328.15	695	1305.31
365	356.56	710	1364.76
380	386.17	725	1425.82
395	416.97	732	1454.87

112

113 The range of the ultrasound water-level is 0 to 792 mm in the channel and the resolution is
114 2 mm. The SSC is estimated using a turbidity probe (*Odeon/Aqualabo*); its accuracy is lower than 5%
115 NTU. Regular cleaning of the probe head is carried out after each flood event. An automatic water
116 sampler (*ISCO 3700*; 24 x 1 L) is used to collect water samples during flood events. The sampler is
117 coupled to the water-level sensor and only operates when water flows through the Venturi channel.
118 All sensors are connected to a data logger (*Ijinus Log0500*). The measured parameters are recorded

every 6 min. Information is downloaded every two weeks on a laptop computer (*Software Avelour 6.0.4*). A tipping-bucket rain gauge (*Précis mécanique; model: 303x*; resolution: 0.2 mm) was also installed in the catchment close to the station (see star symbol in Fig. 1B).

To estimate the SSC over time, 61 water samples were sampled using the automatic water sample. 100 mL of water are filtered in the laboratory using dehydrated cellulose nitrate filters, previously dried in an oven (70°C during 48 h; pore size 0.45 µm). Subsequently, the filters were dried again (70°C during 48 h) and weighed. The weight difference allows evaluating the concentration of the material in the sample. A correlation curve is defined between T the turbidity data (NTU) measured in the field and SSC corresponding to the suspended sediment concentration (g L^{-1}) obtained in the laboratory (Fig. 3).

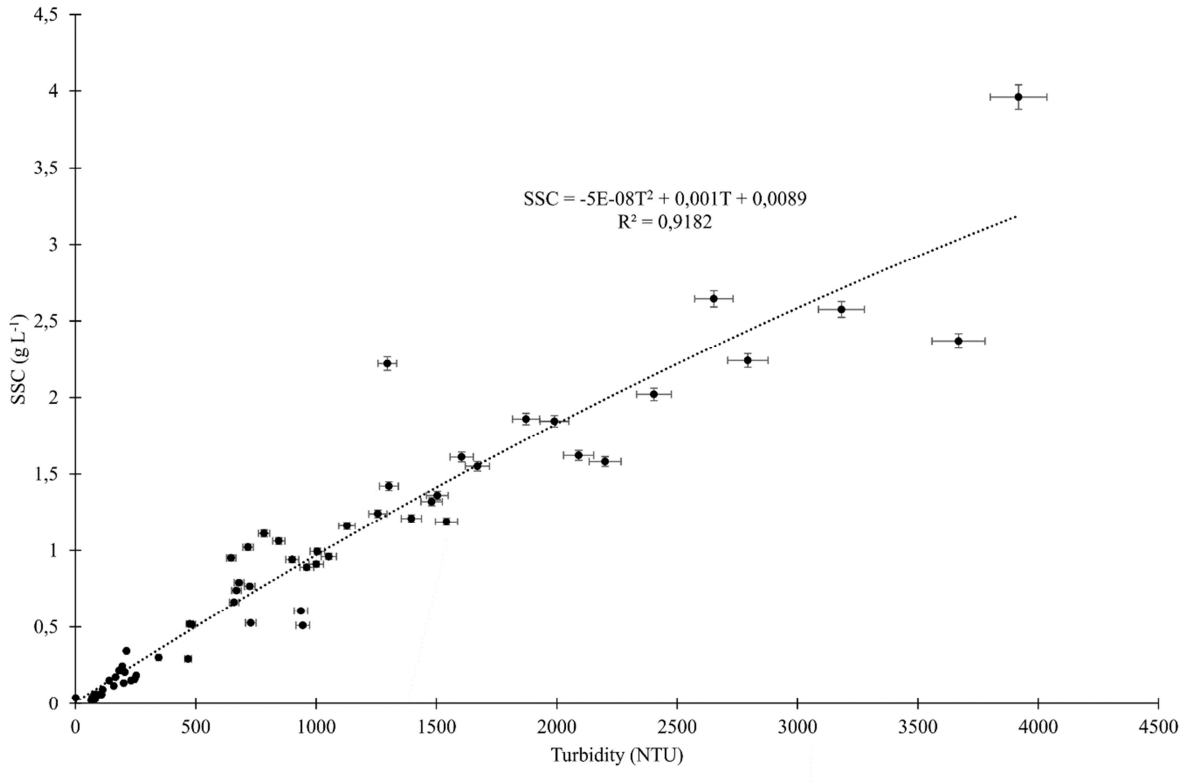

Fig. 3: Correlation curve between turbidity (NTU) and suspended sediment concentration (g L^{-1}) for the water samples sampled in the Venturi channel.

Suspended sediment flux (SSF) is then calculated using Eq. 4:

$$SSF = Q \times SSC \times 10^3 \quad (4)$$

With Q the flow discharge in $m^3\ s^{-1}$ and SSF the instant suspended sediment flux in $g\ s^{-1}$. The sediment yield (SY; in g) is evaluated for each event as (Eq. 5):

$$SY = \int_{t_0}^{t_f} SSF\ dt \quad (5)$$

With t_0 and t_f corresponding to the beginning and the end of the event considered. Then, the SY is converted in kg to facilitate the comparison.

3.2 Analysis of variables

During the two years of monitoring (April 2016 – April 2018), a total of 48 runoff events were recorded. For each event, multiple variables were extracted, related to : (i) duration rainfall event (R_{time}, min), (ii) rainfall amount (Ra, mm), (iii) maximum 6 min rainfall intensity (Ri_{max}, mm h^{-1}), (iv) rainfall amount 48 h before the beginning of the investigated event (Ra_{48}, mm), (v) mean flow and peak flow (Q_{mean}, Q_{max}, $m^3\ h^{-1}$), (vi) mean and maximum SSC concentration (SSC_{mean}, SSC_{max}, $g\ L^{-1}$), (viii) sediment yield (SY, kg), and (ix) total runoff (R_{tot}, m^3). According to Morgan and Duzant (2008) rainfall detachment is better reflected by rainfall kinetic energy (RKE, $J\ m^{-2}\ mm^{-1}$) than by rainfall intensity, thus the RKE was derived from the Ri_{max} value using the equation of Brandt (1989; Eq. 6), that was tested in the similar environmental context of the Loire River watershed in France (Grangeon et al., 2017):

$$RKE = 8.95 + 8.44 \times \log_{10} Ri_{max} \quad (6)$$

The rainfall erosivity index (EI_{30}) was also considered as it measures both rainfall's kinetic energy and intensity to describe the effect of rainfall on sheet and rill erosion (Wischmeier and Smith, 1978). It is a product of kinetic energy of a rainfall event (E) and its maximum 30-min intensity (I_{30}). The rainfall erosivity index (EI_{30}; MJ mm $ha^{-1}\ h^{-1}$) was calculated for each event using the Eq. 7 given by Brown and Foster (1987):

$$EI_{30} = \left(\sum_{r=1}^{m} e_r \times v_r\right) \times I_{30} \quad (7)$$

154

155 Where e_r is the unit rainfall energy (MJ ha^{-1} mm^{-1}) and v_r is the rainfall volume (mm) during
156 the r-th period, divided into m parts. I_{30} is the maximum rainfall intensity during a 30-min period of
157 the rainfall event (mm h^{-1}). I_{30} is evaluated using the high-resolution rainfall data (6 min) which
158 provides better EI_{30} values according to Panagos et al. (2015b).

159 The unit rainfall energy e_r is calculated for each time interval as follows (Brown and Foster,
160 1987):

$$e_r = 0.29 \times [1 - (0.72 \times e^{-0.05 \times i_r})] \quad (8)$$

161

162 Where i is the rainfall intensity during the time interval (mm h^{-1}).

163 *3.3 Pearson correlation matrix and Principal Component Analysis (PCA)*

164 Statistical analyses were performed using the statistical software *R*[1] and the following
165 packages: *FactoMiner*[2] and *Corrplot*[3]. Pearson correlation matrix is used to evaluate the linear
166 dependency between multiple variables simultaneously. The result is given using the Pearson
167 correlation coefficient r which reflects the linear correlation between two variables. The coefficient is
168 calculated using the covariance of two variables divided by the product of their standard deviations
169 (Eq. 9):

$$r = \frac{\sum_{i=1}^{n}(x_i - \bar{x})(y_i - \bar{y})}{\sqrt{\sum_{i=1}^{n}(x_i - \bar{x})^2}\sqrt{\sum_{i=1}^{n}(y_i - \bar{y})^2}} \quad (9)$$

170

[1] R Core Team (2016). R: A Language and Environment for Statistical Computing. R Foundation for Statistical Computing, Vienna, Austria. URL https://www.R-project.org/.
[2] https://cran.r-project.org/web/packages/FactoMineR/index.html
[3] https://cran.r-project.org/web/packages/corrplot/index.html

Where n is the sample size; x_i and y_i are the values of the sample; $\bar{x}$ and $\bar{y}$ are the mean values of the sample. A value of 1 implies that a linear equation describes the perfect relationship between x_i and y_i, with all data points lying on a line for which y_i increases as x_i increases. A value of −1 implies that all data points lie on a line for which y_i decreases as x_i increases. A value of 0 implies that there is no linear correlation between the variables.

3.4 General characteristics of runoff events

3.4.1 First year of monitoring

Between April 2016 and April 2017, 22 runoff events were recorded: seven occurred in spring, three in summer, four in autumn, and eight in winter. The main characteristics of these events are summarized in Table 2 and are described in detail in the following text:

i. The duration of runoff events ranged from 126 to 7200 min in total with a median value of 534 min. Five events (22%) showed a duration longer than 1000 min, and five events (22%) correspond to shorter period (less than 360 min), one event exceeded 2000 min.

ii. The rainfall amount ranged from 6 to 103.8 mm with a median value of 16.1. Eight events (36%) exceeded 20 mm, and five events (22%) had values lower than 10 mm.

iii. The maximum 6 min rainfall intensity ranged from 3 to 76 mm h^{-1}, and three events (13%) exceeded 20 mm h^{-1}. The amount of precipitation 48 h before the beginning of an event ranged from 0.2 to 25.4 mm. Seven events (32%) showed a rainfall amount 48 h before the beginning of an event that was higher than 10 mm.

iv. The peak flow ranged from 0.6 to 378.3 m^3 h^{-1} and the mean flow ranged from 0.11 to 94.5 m^3 h^{-1}. Ten events (45.5%) showed values of a peak flow exceeding 100 m^3 h^{-1}.

v. The maximum SSC ranged from 0.15 to 5 g L^{-1} and the mean SSC ranged from 0.06 to 1.6 g L^{-1}. Eleven events (50%) showed values of maximum SSC exceeding 3 g L^{-1}.

vi. The sediment yield values ranged from 0.07 to 7131.9 kg and were extremely variable. Three events (13.6%) exceeded 1500 kg and one event exceeded 2500 kg. This event represents 44.8% of the total sediment discharge for the first year of monitoring.

vii. The total runoff ranged from 0.57 to 8630.5 m^3. Four events (18.2%) exceeded 1000 m^3 and one event exceeded 2500 m^3.

viii. The rainfall kinetic energy ranged from 13 to 24.8 J m^{-2} mm^{-1}. Events with a high RKE (> 20) are mainly observed during the spring season, and do not correspond to the events with the highest sediment yield recorded at the outlet.

ix. The rainfall erosivity index (EI_{30}) ranged from 0.7 to 236.2 MJ mm ha^{-1} hr^{-1} with a mean value of 25.3 MJ mm ha^{-1} hr^{-1}. Highest value of EI_{30} is observed in May (236.2 MJ mm ha^{-1} hr^{-1}) during an intensive rainfall event where Ri_{max} reached 76 mm h^{-1}. The sum of EI_{30} during the first year of monitoring round up to 557.45 MJ mm ha^{-1} hr^{-1}.

Table 2: Main characteristics of the 22 flood events recorded in the Pommeroye catchment between April 2016 and April 2017.

Date	R_{time} (min)	Ra (mm)	Ri_{max} (mm h^{-1})	Ra_{48} (mm)	Q_{mean} (m^3 h^{-1})	Q_{max} (m^3 h^{-1})	SSC_{mean} (g L^{-1})	SSC_{max} (g L^{-1})	SY (kg)	R_{tot} (m^3)	RKE (J m^{-2} mm^{-1})	EI_{30} (MJ mm ha^{-1} hr^{-1})
12-Apr-16	192	8.1	9	5.8	15	42	1.2	4.1	71.2	31.4	17	4.3
15-Apr-16	366	13.8	12	0.6	5.9	10.8	0.4	2.1	5.8	8.2	18.1	6.5
11-May-16	288	32.6	76	7.2	22.2	150.8	1.6	5	652.7	186.5	24.8	236.2
22-May-16	204	9.8	6	2.8	0.25	0.6	0.06	0.15	0.07	0.8	15.5	3.5
31-May-16	1110	30.6	14	0.2	22.6	147	0.7	3	235.8	106.2	18.6	9.7
3-Jun-16	126	6	12	1.4	1.91	6.24	0.13	0.8	1.4	4.6	18.1	4.8
20-Jun-16	372	8.7	3	3.4	3.7	9.14	0.1	0.27	4.3	23.3	13	5.2
23-Jun-16	245	12.9	21	5.3	13.6	60.7	0.5	2.69	80.2	69.3	20.1	42
2-Aug-16	1968	68.6	10	18.4	12.4	108.6	0.32	4.58	590.9	407.5	17.4	39.1
9-Sep-16	324	27	24	0.2	4.5	6.2	0.5	2.7	6.8	12.2	20.6	50.8
20-Oct-16	390	16.6	4	11.4	3.08	12.9	1.06	4.03	30.4	20.3	14	3.9
7-Nov-16	1434	17.5	8	0.9	0.11	0.99	0.5	3.02	0.6	0.57	16.6	8.2
16-Nov-16	540	9.7	3	1.2	0.34	2.54	0.38	1.63	1.86	3.7	13	3.8
17-Nov-16	7200	103.8	18	10.9	75.2	378.3	0.41	4.02	7131.9	8630.5	19.5	83.5
12-Jan-17	528	22	12	2	55.18	190.9	1.35	4.9	1597.6	772.6	18.1	16.1
4-Feb-17	432	6.8	6	11.8	1.96	13.7	0.12	0.89	8.99	16.2	15.5	1.32
5-Feb-17	702	25.2	6	11.8	94.5	235.8	0.74	3.7	2119.7	1767.4	15.5	8.43
7-Feb-17	804	10.6	8	25.4	34.4	209.8	0.37	3.4	627.3	561.3	16.6	4.8
27-Feb-17	852	15.6	8	1	3.9	37.5	0.42	3.7	87.9	57.9	16.6	0.7
28-Feb-17	1002	21.6	8	17	68.4	221.8	0.35	1.59	991.3	1957.1	16.6	9.4
5-Mar-17	1050	16.8	10	11.4	36.1	227.9	0.35	3.82	1059.5	1274.6	17.3	10.5
8-Mar-17	894	14.6	4	0.6	50.8	189.5	0.19	1.27	595.1	2031.8	14	4.7
Mean	955.6	22.7	12.8	6.9	23.9	102.9	0.54	2.8	722.8	815.6	17.1	25.3
Std dev.	1467.2	22.6	15.2	7	28	108.4	0.42	1.5	1544.9	1873.3	2.7	51.4

3.4.2 Second year of monitoring

Between April 2017 and April 2018, 26 runoff events were recorded: twelve events occurred in autumn and fourteen in winter. The main characteristics of these events are summarized in Table 3 and are described in detail in the following text:

i. The duration of runoff events ranged from 72 to 4098 min in total with a median value of 522 min. Eight events (30%) showed a duration longer than 1000 min, and seven events (27%) correspond to shorter flooding (less than 360 min).

ii. The rainfall amount ranged from 2 to 55.2 mm with a median value of 12.2 mm. Eight events (30%) show values over 20 mm, and eleven events (42%) were lower than 10 mm.

iii. The maximum 6 min rainfall intensity ranged from 1 to 32 mm h^{-1} and five events exceeded 20 mm h^{-1}. 48 h-antecedent rainfalls ranged from 0 to 31.8 mm and twelve events (46%) showed 48 h-antecedent rainfalls higher than 10 mm.

iv. The peak flow ranged from 60.4 to 348.6 m^3 h^{-1} and the mean flow ranged from 14.7 to 110.1 m^3 h^{-1}. 24 events (92%) showed a value of peak flow exceeding 100 m^3 h^{-1}.

v. The maximum SSC range from 0.5 to 5 g L^{-1} and the mean SSC ranged from 0.08 to 1.31 g L^{-1}. Twelve events (46%) showed values of maximum SSC exceeding 3 g L^{-1}.

vi. The sediment yield values ranged from 54.8 to 7577.5 kg. Nine events (34%) exceeded 1500 kg and three main events (11%) exceeded 3000 kg.

vii. The total runoff ranged from 141 to 5255.5 m^3. Eleven events exceeded 1000 m^3 and two main events exceeded 2500 m^3.

viii. The rainfall kinetic energy ranged from 8.9 to 21.7 J m^{-2} mm^{-1} and show a biggest variability than the previous year. Highest RKE are principally observed between October and December 2017.

ix. The rainfall erosivity index (EI_{30}) ranged from 0.9 to 81.8 MJ mm ha^{-1} hr^{-1} with a mean value of 12.5 MJ mm ha^{-1} hr^{-1}. The sum of EI_{30} during the first year of monitoring

237 round up to 314.15 MJ mm ha^{-1} hr^{-1}, which is considerably lower than the previous

238 year.

239 **Table 3: Main characteristics of the 26 flood events recorded in the Pommeroye catchment between April 2017 and April 2018.**

Date	R_{time} (min)	Ra (mm)	Ri_{max} (mm h^{-1})	Ra_{48} (mm)	Q_{mean} (m^3 h^{-1})	Q_{max} (m^3 h^{-1})	SSC_{mean} (g L^{-1})	SSC_{max} (g L^{-1})	SY (kg)	R_{tot} (m^3)	RKE (J m^{-2} mm^{-1})	EI_{30} (MJ mm ha^{-1} hr^{-1})
20-Oct-17	600	4.8	6	1.3	16.9	74.6	0.11	1.3	54.8	211	15.5	0.9
22-Oct-17	600	28.9	32	7.8	20	170	0.17	2.2	167.1	210	21.7	11.8
23-Oct-17	966	7.1	1	28.9	14.7	60.4	0.08	0.5	55.7	461	8.9	1.3
14-Nov-17	2292	5.6	6	0.5	17.7	144.8	0.12	1.8	200.5	670	15.5	1.7
18-Nov-17	72	15.2	10	0.8	27.5	183.1	0.24	2.4	137.3	184	17.4	8.7
20-Nov-17	822	23.2	8	19	33.3	140	0.26	2.3	300.9	786	16.6	12
27-Nov-17	2238	54.8	24	0.2	56.5	308.5	0.59	4.1	3529	2234	20.6	81.8
29-Nov-17	1158	14.6	10	6.8	36	153	0.3	5.0	354.8	659	17.4	8.95
7-Dec-17	498	8.8	6	0.6	24.8	177.2	0.22	3.2	120.2	141	15.5	1.4
10-Dec-17	1338	14.4	10	0	46.6	348.6	0.48	4.0	1799	961	17.4	5.4
11-Dec-17	1218	20.4	6	14.4	28	285	0.23	4.2	1064.2	1186	15.5	6.6
13-Dec-17	4098	55.2	8	20.6	64.9	325.9	0.67	4.3	7577.5	5255.5	16.6	25.5
27-Dec-17	372	5.2	4	6	48.1	117.7	0.45	3.4	311.3	442.5	14	0.9
29-Dec-17	420	15	22	3	91.2	321.5	1.03	4.3	2239.8	1177.1	20.3	25.6
30-Dec-17	366	6.2	4	15.4	54.5	172	0.52	2.2	677.7	807	14	1.3
31-Dec-17	2694	37.2	30	21.4	80.8	335.7	0.89	3.8	6919.7	4245.1	21.4	62.6
3-Jan-18	192	10.4	10	17.2	110.1	294.4	1.31	3.1	3084.4	1357.3	17.4	6.9
4-Jan-18	336	21.2	6	13.6	86.9	239.5	0.99	3.2	2353.1	1286.9	15.5	7.8
5-Jan-18	360	8	20	31.8	73.1	328.3	0.79	4.3	1886.5	1104.8	19.9	13
6-Jan-18	330	7.4	14	29.8	55.8	235.9	0.56	1.9	796.6	725.9	18.6	7
15-Jan-18	546	14	6	0.2	98.7	229	1.11	3	874.7	622.3	15.5	4.7
18-Jan-18	408	10	4	3	91.1	178.5	0.99	2.9	645.2	573.6	14	2.2
21-Jan-18	1062	26	6	11.4	71.4	258.7	0.77	3.5	2096.7	1435.7	15.5	9
23-Jan-18	408	2	2	4.8	35.5	156.9	0.31	2.8	161.3	230.7	11.5	0.4

31-Jan-18	306	5.8	8	7.6	72.3	265.4	0.79	2.3	823.8	571.3	16.6	5.3
1-Feb-18	174	4.2	6	12.4	45.71	91.4	0.39	1.9	99.1	196.5	15.5	1.4
Mean	918.2	16.3	10.3	10.7	53.9	215.3	0.55	2.99	1474.2	1066.7	16.5	12.5
Std dev.	944.6	14.2	8.3	9.8	28.1	86.9	0.35	1.08	1970.2	1198.4	2.9	18.9

4 Results

4.1 Relationships between variables

To identify the factors that may explain the measured hydro-sedimentological response at the outlet of the Pommeroye catchment, a Pearson correlation matrix was generated from all collected parameters. The results show significant correlations between the rainfall variables and the hydro-sedimentary response of the catchment area (Fig. 4). The highest relationship was found between the sediment yield (SY) and the total runoff (R_{tot}; r = 0.91). Strong correlations were observed between the duration time of the event (R_{time}), rainfall amount (Ra), and sediment yield (r = 0.76; r = 0.68). Reasonable correlations exist between the discharge variables (Q_{mean}, Q_{max}), sediment yield (SY) and total runoff (R_{tot}) (r = 0.72; r = 0.65; r = 0.59; r = 0.5, respectively). A relationship between rainfall kinetic energy (RKE), rainfall erosivity index (EI_{30}) and the maximum suspended sediment concentration (SSC_{max}) is also observed (r = 0.54; r = 0.42).

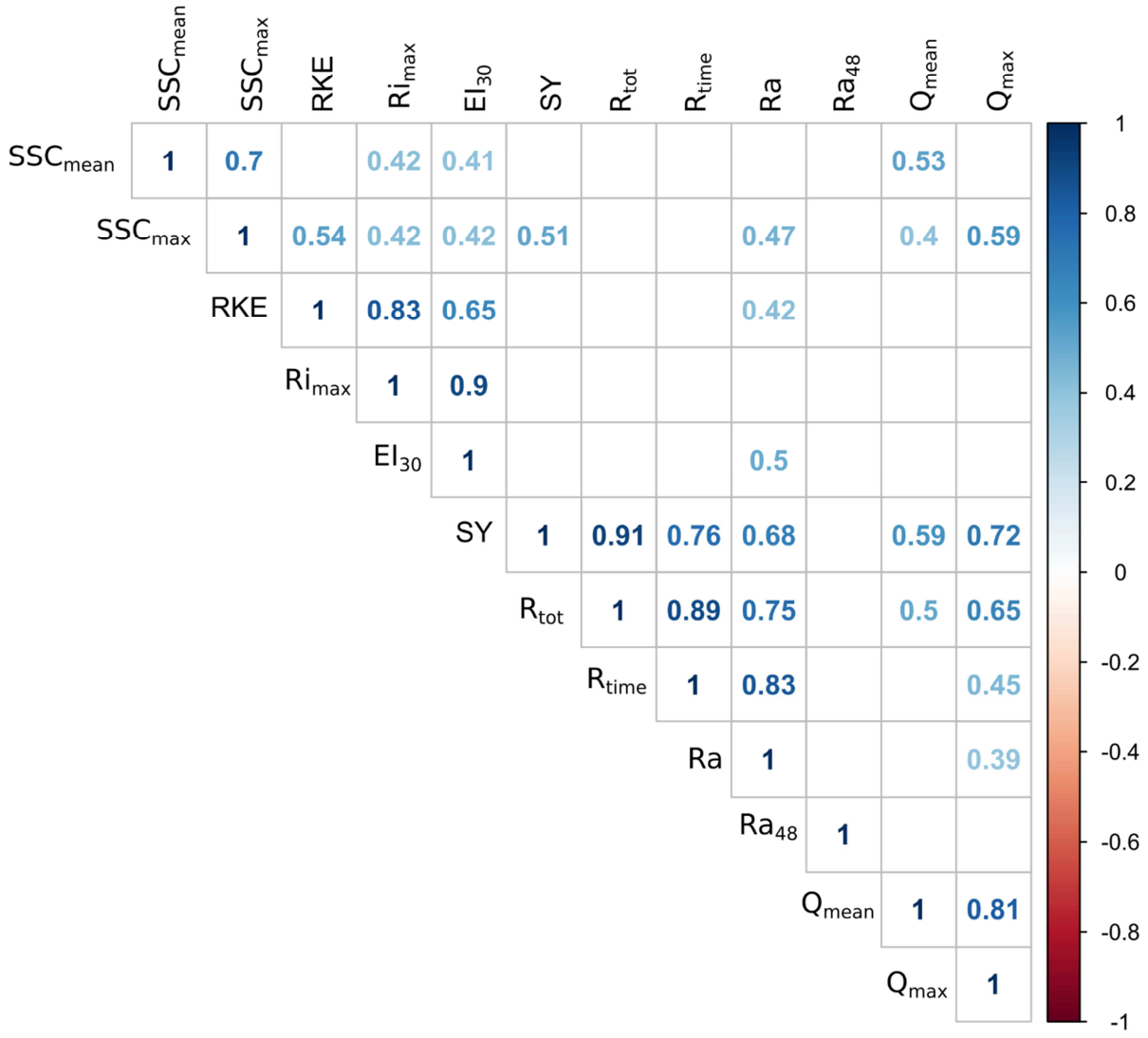

Fig. 4: Pearson correlation matrix between all variables (n=48 events). Coefficient r is considered significant at p = 0.01.

Excellent correlations were found between sediment yield and the maximum and mean flow discharge (r^2= 0.91 and r^2 = 0.84, respectively; Fig. 5A and B) even with a dispersion for the biggest runoff events. The relationship between sediment yield and rainfall amount is statistically significant (r^2 = 0.46), although it shows a wide scatter in the data (Fig. 5C). The maximum sediment yield at the outlet is observed when the rainfall amount exceeds 36 mm, except for one event occurring in summer 2016. Below the threshold of 36 mm, rainfall amount results in a more variable sediment yield at the outlet. For example, a rainfall amount of 15 mm results in a sediment yield varying between 50 and 2300 kg. The relationship between the peak flow and the maximum suspended

sediment concentration was not statistically significant ($r^2 = 0.20$). For a 4 g L^{-1} suspended sediment concentration the resulting peak flow varied between 10 and 380 $m^3 h^{-1}$ suggesting that the relationships between these two variables is more complex (Fig. 5D). The 48 h-antecedent rainfall does not show significant statistical relationships with the hydro-sedimentary response.

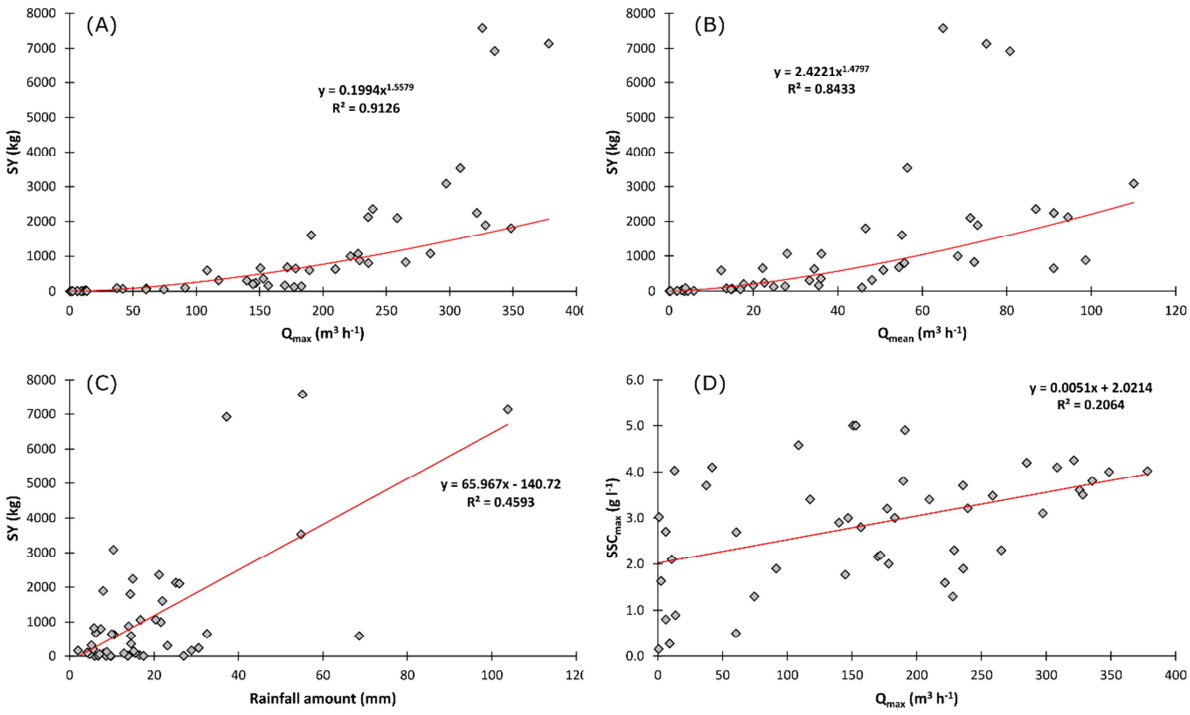

Fig. 5: Relationship between (A) sediment yield (kg) and the maximum flow discharge ($m^3 h^{-1}$), (B) sediment yield (kg) and the mean flow discharge ($m^3 h^{-1}$), (C) sediment yield (kg) and the rainfall amount (mm), and (D) the maximum suspended sediment concentration (g L^{-1}) and the maximum flow discharge ($m^3 h^{-1}$) after two years of monitoring in the Pommeroye catchment.

4.2 Sediment production variability

4.2.1 First year of monitoring

From April 2016 to April 2017, the total SY recorded at the monitoring station reached 15901 kg (Fig. 6 and Fig. 7). The cumulated rainfall reached 827.1 mm, which is relatively low for the area (mean annual cumulative rainfall = 1000 ± 150 mm yr^{-1}). Normalized to the catchment area (0.54 km^2), the specific sediment yield (SSY) reached 29.4 t km^{-2} yr^{-1}. The sediment yield shows a high heterogeneity between the different seasons. The seasonal SY, compared to annual SY in % is: (i)

971 kg in spring (6.1%), (ii) 678 kg in summer (4.3%), (iii) 7165 kg in autumn (45%), and (iv) 7087 kg in winter (44.6%).

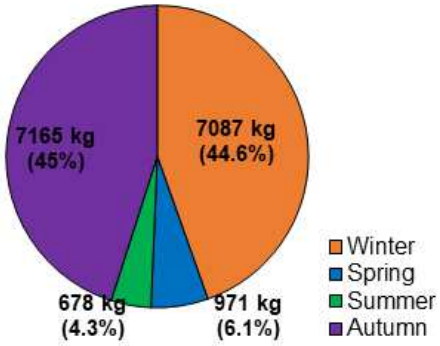

Fig. 6 : Seasonal distribution of the sediment export (%) at the outlet of the Pommeroye catchment for the first year of monitoring (April 2016 – April 2017).

In spring 2016, seven events contributed to the SY. Over this period, the total rainfall was 191 mm. The event of May 11, 2016 had the highest impact with a SY of 658 kg following a cumulative rainfall of 32.6 mm. This event contributed to 68% of the seasonal SY for spring. This may be explained by the fact that high rainfall intensities were measured, reaching up to 76 mm h^{-1} and high value for the RKE (24.8 J m^{-2} mm^{-1}). For this event, maximum SSC was observed with a value of 5 g L^{-1}.

In summer 2016, three events were recorded. Over this period, the total rainfall was 201.2 mm. On August 02, 2016 a SY of 591 kg and high cumulative rainfall (68.6 mm) was observed. This event contributed to 87% of the seasonal SY for summer 2016. Unlike during the spring season, rainfall intensities observed in summer were much lower. They reached 21mm h^{-1} for the event on August 02, 2016. This explains why the observed SY is different between these two seasons.

In autumn 2016, four events were recorded including a peak event. Over this period, the total rainfall was 195.9 mm. The event of November 17, 2016 was due to a cumulative rainfall of 103.8 mm over five days. The SY for this event reached 7132 kg, equivalent to 45% of the total SY for

298 the entire year. The maximum rainfall intensity was relatively high (18 mm h^{-1}) but lower than in the
299 previous seasons.

300 Winter 2016/2017 was the season with the highest frequency of rainfall events. A total of
301 eight events were reported. Over this period, the total rainfall was 239 mm. The events of
302 January 15, 2017 and February 02, 2017 contributed to 3717 kg (52.5%) of the total SY for winter
303 season. These two events are the result of cumulative rainfalls of 22 and 25.2 mm, respectively. Four
304 other events contributed to 3273 kg (46%) of the total SY in winter season. These events correspond
305 to cumulative rainfall that ranged from 10.6 to 21.6 mm. During this period, lower heterogeneity
306 between the events was observed, due to an almost equivalent cumulative rainfall for the different
307 events and rainfall intensities that are generally low (between 4 to 12 mm h^{-1}).

308 Over the entire first year of monitoring, it is noteworthy that during spring period, the
309 highest sediment concentration was observed at the outlet. The autumn and winter seasons
310 contributed equally to the total SY measured but strong heterogeneities between rainfall events was
311 observed.

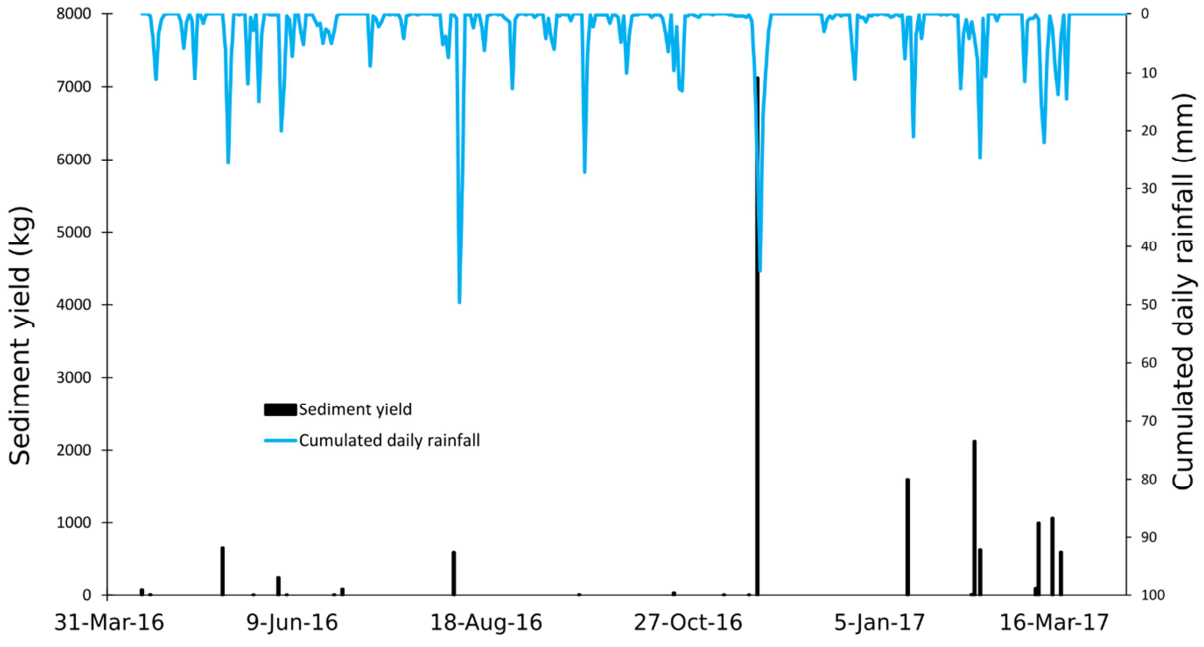

312

Fig. 7: Sediment yield (kg) and cumulative daily rainfall (mm) recorded at the outlet of the Pommeroye catchment during the first year of monitoring (April 2016- April 2017).

4.2.2 Second year of monitoring

From April 2017 to April 2018, the total SY recorded at the monitoring station reached 38330 kg (Fig. 8 and Fig. 9). The cumulated rainfall reached 965.8 mm which is higher than previous year. Normalized by the catchment area (0.54 km²), the SSY reached 70 t km^{-2} yr^{-1}. The seasonal SY, compared to annual SY in % is: (i) 15361 kg in autumn (40%) and (ii) 22969 kg in winter (60%). The two other seasons are not represented here as no events were recorded at the monitoring station.

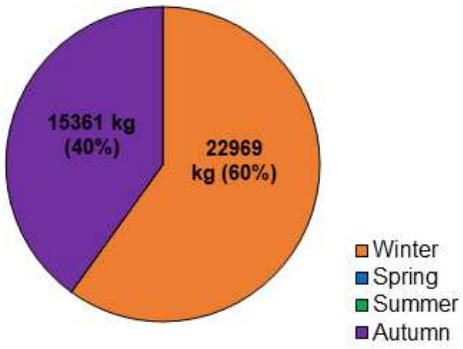

Fig. 8: Seasonal distribution of the sediment export (%) at the outlet of the Pommeroye catchment for the second year of monitoring (April 2017 – April 2018).

In autumn 2017, twelve events were recorded for a total rainfall of 367.5 mm, thus 171.6 mm more than during the previous year for the same season. Two events contributed to 72% of the seasonal SY for autumn 2017. For the event of November 27, 2017, the measured SY can be explained by a high rainfall amount (54.8 mm) and the highest maximum rainfall intensity recorded for this season (24 mm h^{-1}). For the event on December 13, 2017, the rainfall amount was similar (55.2 mm) but the maximum rainfall intensity was lowest (8 mm h^{-1}). The observed SY can be explained by a long duration of the rainfall event (3 days) and a high amount of 48 h-antecedent rainfall (20.6 mm).

In winter 2017/2018, fourteen events were recorded for a total rainfall of 323.2 mm, thus 84.2 mm more than in the previous year for the same season. 74% of the seasonal SY was produced

between December 29, 2017 and January 5, 2018. The main event of December 31, 2017 which contributed to 30% showed the longest duration of rainfall event (2694 min). The rainfall amount was 37.2 mm with a high maximum rainfall intensity (30 mm h^{-1}) and a high amount of 48 h-antecedent rainfall (21.4 mm). The events following this main event were of relatively short rainfall event duration between 192 and 420 min. The rainfall amount was variable and comprised values between 5.2 and 21.2 mm, just as the maximum rainfall intensity, which varied between 4 and 22 mm h^{-1}.Five events were characterized by a high amount of 48 h-antecedent rainfall varying between 13.6 and 29.8 mm. After January 15, 2018, six more events were recorded. They contributed to 20% to the seasonal SY with a rainfall amount ranges from 2 to 26 mm and durations between 174 and 1062 min. Rainfall intensity were relatively low from 2 to 8 mm h^{-1} and the 48 h-antecedent rainfall ranged from 0.2 to 12.4 mm.

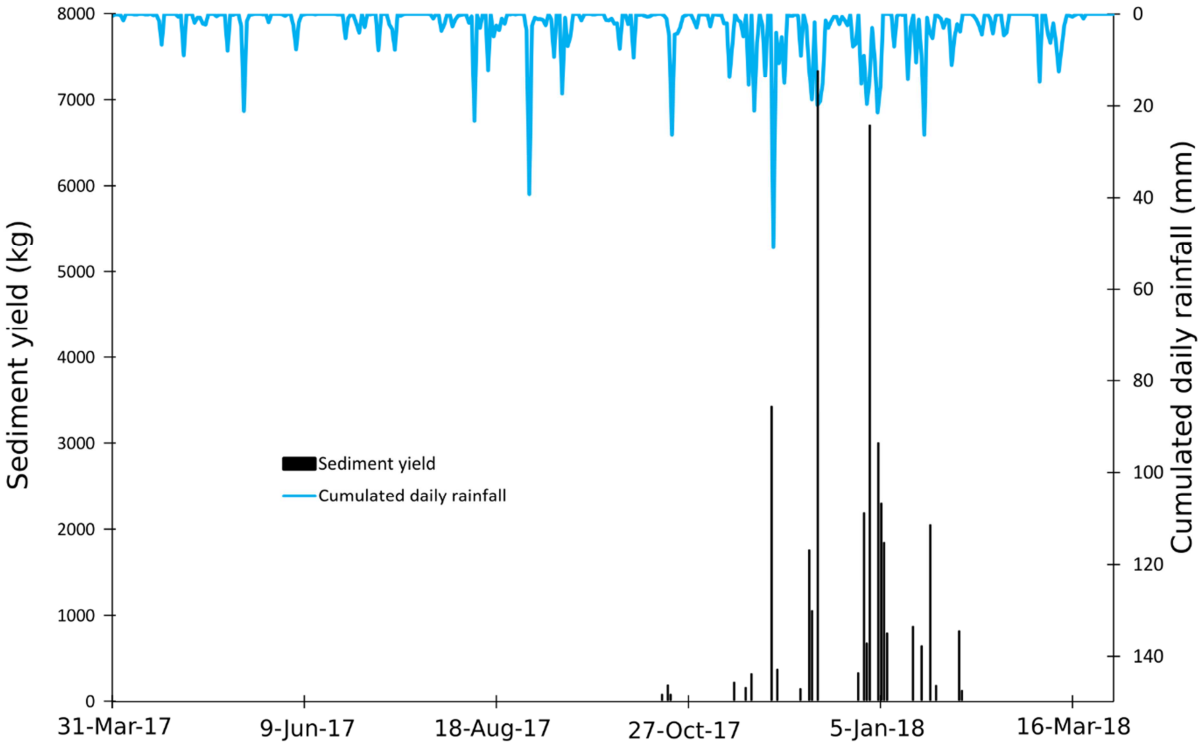

Fig. 9: Sediment yield (kg) and cumulative daily rainfall (mm) recorded at the outlet of the Pommeroye catchment during the second year of monitoring (April 2017 - April 2018).

348 *4.3 Seasonal variability*

349 The eigen-values (Table 4) provide the percentage of the explained variance and the
350 cumulative variance of the principal dimensions. The first three dimensions explain 79.2% of the total
351 variance: dimension 1 accounts for 44.2%, dimension 2 for 20.5%, and dimension 3 for 14.5%. The
352 square cosines of variables indicate the best-described variables on each principal dimension.
353 Dimension 1 is correlated to R_{time} (0.48), Ra (0.59), Q_{max} (0.59), SSC_{max} (0.54), SY (0.76), and R_{tot} (0.66).
354 Dimension 2 is correlated to Ri_{max} (0.61), RKE (0.40), and EI_{30} (0.40). Dimension 3 is correlated to
355 Q_{mean} (0.40) and SSC_{mean} (0.36). Ra_{48} is correlated to Dimension 4 (0.72) which represented only 7.2%
356 of the total variance. The bi-plot graphs (Fig. 10 and Fig. 11) allow visualizing the information on
357 both, individual samples and variables.

358 **Table 4: Eigen-values, percentages of variance explained, and cumulative variance of principal dimensions for**
359 **the principal component analysis.**

	Eigen-value	Percentage of explained variance (%)	Cumulative percentage of explained variance (%)
Dim 1	5.3	44.2	44.2
Dim 2	2.46	20.5	64.7
Dim 3	1.75	14.5	79.2
Dim 4	0.87	7.2	86.4
Dim 5	0.57	4.8	91.2
Dim 6	0.45	3.8	95
Dim 7	0.24	2	97
Dim 8	0.19	1.5	98.5
Dim 9	0.08	0.7	99.2
Dim 10	0.04	0.4	99.6
Dim 11	0.03	0.2	99.8
Dim 12	0.02	0.2	100

360

361 In the first space Dim1-Dim2, we observe a classification between the different events
362 (Fig. 10). On $Dim1^{+}/Dim2^{+}$, a minority of events are represented and are those characterized with the
363 highest values of the following parameters: Ri_{max}, RKE, EI_{30}, SSC_{mean}, SSC_{max}. These events are the most
364 erosive and occurred in the four seasons. The event of May 11, 2016 seems to have a high influence
365 on the projection of the principle component analysis (PCA) due to a high value of climatic

366 parameters. This event was the most erosive with very high rainfall intensities (76 mm h^{-1}) and a
367 strong erosivity power (RKE = 24.8 J m^{-2} mm^{-1}; EI_{30} = 236.2 MJ mm ha^{-1} h^{-1}), which results on a high
368 suspended sediment concentration at the outlet of the catchment. Nevertheless, these events are
369 not characterized by the highest sediment yield at the outlet. Events with the highest values for flow
370 discharge and sediment yield are represented in $Dim1^{+}/Dim2^{-}$ and occurred mostly in autumn and
371 winter. These events are characterized by the highest values of sediment yield induced by highest
372 values of rainfall characteristics (Ra, R_{tot}, R_{time}). In the two other spaces ($Dim1^{-}/Dim2^{+}$; $Dim1^{-}/Dim2^{-}$),
373 the events occurred mainly in winter, spring, and autumn. As there is no discriminating parameter on
374 this side, these events are characterized by the lowest values of the different parameters previously
375 cited.

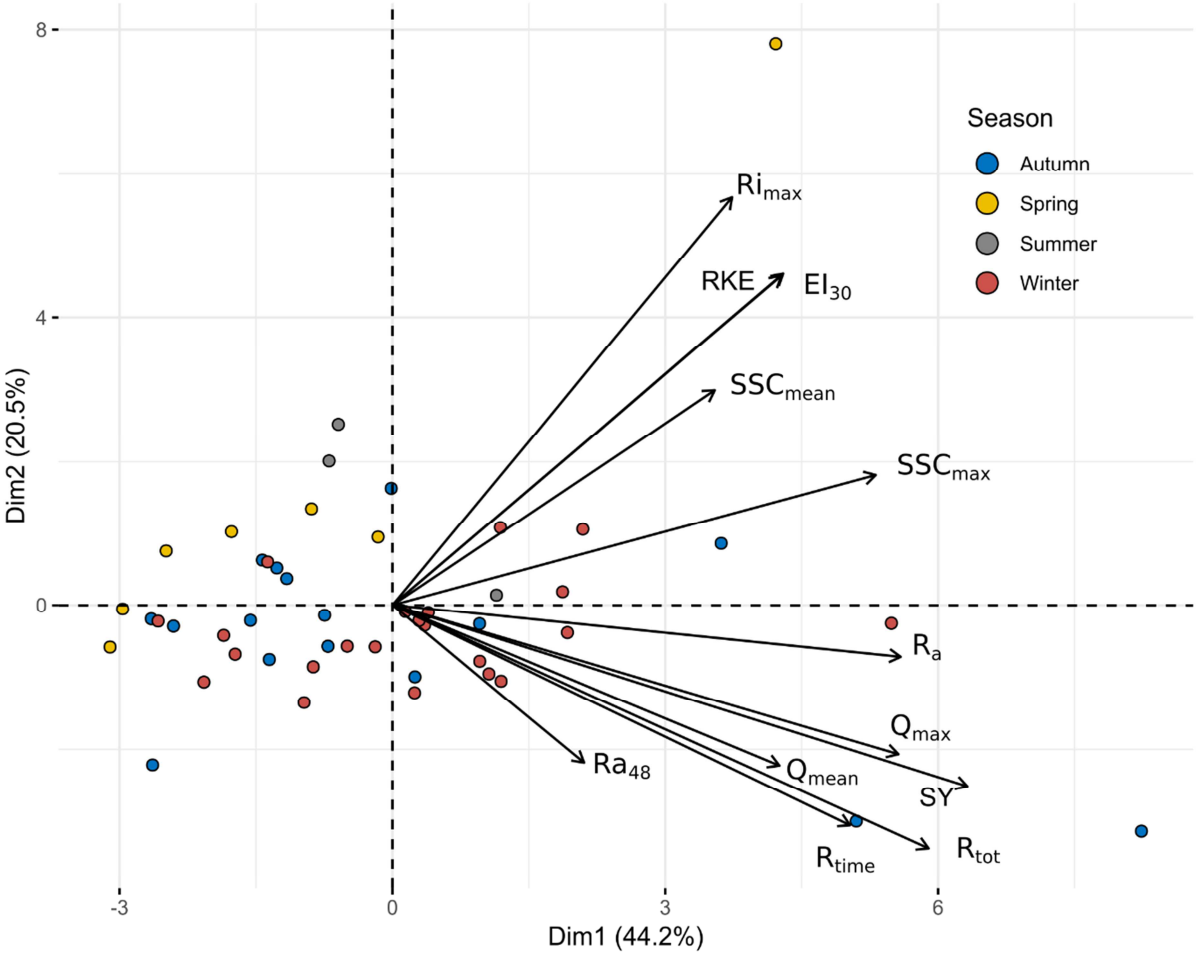

376

377 **Fig. 10: Bi-plot of PCA results on dimensions 1-2 for the 48 events and their hydro-sedimentary parameters: (i)**
378 **duration of the rainfall event (R_{time}, min), (ii) rainfall amount (Ra, mm), (iii) max 6 min rainfall intensity (Ri_{max}, mm h^{-1}),**
379 **(iv) 48 h-antecedent rainfall (Ra_{48}, mm), (v) mean flow and peak flow (Q_{mean}, Q_{max}, m^3 h^{-1}), (vi) mean and maximum SSC**
380 **concentration (SSC_{mean}, SSC_{max}, g L^{-1}), (viii) sediment yield (SY, kg), (ix) total runoff (R_{tot}, m^3), (x) rainfall kinetic energy**
381 **(RKE, J m^{-2} mm^{-1}), and (xi) rainfall erosivity index (EI_{30}, MJ mm ha^{-1} h^{-1}).**

382 In the second space Dim1/Dim3, the classification of the events shows some additional
383 information (Fig. 11). A major part of the winter events is represented in the $Dim1^+/Dim3^+$ space and
384 is characterized by high values of Q_{mean}, Q_{max}, SSC_{mean}, and SSC_{max}. In this space, the parameter Ra_{48}
385 appears to be discriminating. In $Dim1^+/Dim3^-$, few events of the season autumn, spring, and summer
386 are represented. They are characterized by the highest values of SY, EI_{30}, Ri_{max}, Ra, RKE, and R_{time}.
387 However, most of the events occurring in these three seasons are represented in the space $Dim1^-$
388 $/Dim3^-$ and are largely influenced by the value of the previously citer parameters.

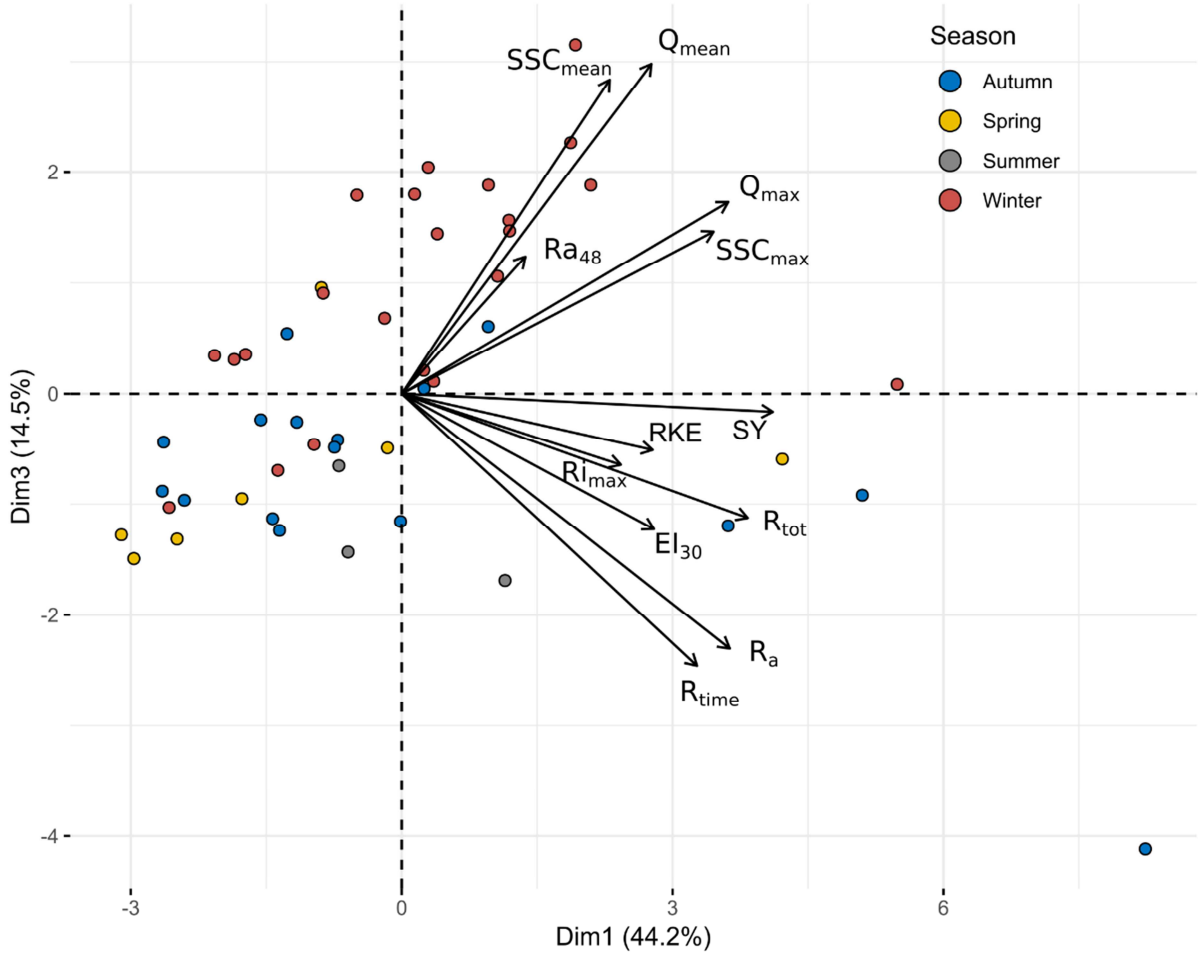

389

390 **Fig. 11: Bi-plot of PCA results on dimensions 1-3 for the 48 events and their hydro-sedimentary parameters: (i)**
391 **duration of the rainfall event (R_{time}, min), (ii) rainfall amount (Ra, mm), (iii) max 6-min rainfall intensity (Ri_{max}, mm h^{-1}),**
392 **(iv) 48 h-antecedent rainfall (Ra_{48}, mm), (v) mean flow and peak flow (Q_{mean}, Q_{max}, m^3 h^{-1}), (vi) mean and maximum SSC**
393 **concentration (SSC_{mean}, SSC_{max}, g L^{-1}), (viii) sediment yield (SY, kg), (ix) total runoff (R_{tot}, m^3), (x) rainfall kinetic energy**
394 **(RKE, J m^{-2} mm^{-1}), and (xi) rainfall erosivity index (EI_{30}, MJ mm ha^{-1} h^{-1}).**

395 ## 5 Discussion

396 A high intra-annual variability of the hydro-sedimentary response is observed at the outlet of
397 the Pommeroye catchment. The experimental station measured a specific sediment yield between
398 29.4 and 70 t km^{-2} yr^{-1} over two years of monitoring while the intra-annual variability of cumulative
399 rainfall is low with a difference of 138.7 mm. The high variability of the hydro-sedimentary response
400 is explained by the 48 erosive events recorded which show a strong heterogeneity. Sediment flux for
401 a single event ranges from 0.6 to 7131.8 kg, with an average of 722.8 kg. The total runoff between
402 discrete events also shows strong variations ranging from 0.57 to 8630.5 m^3. This variability of the

403 hydro-sedimentary response can be mainly explained by different types of rainfall events.
404 Cumulative rainfall for a single event shows a high variability (i.e. from 2 to 103.8 mm) as well as the
405 recorded maximum rainfall intensities (i.e. from 2 to 76 mm h^{-1}).

406 The amount of exported sediment is consistent with values observed in similar studies areas.
407 The specific sediment yield is higher than those observed by Grangeon et al. (2017) across the main
408 Louroux subcatchments (France) where sediment fluxes varied from 1 to 38 t km^{-2} yr^{-1}. Our results on
409 SY are also higher than those published by Lefrançois (2007) for the French catchments of the
410 Moulinet and the Violettes (i.e. 25.4 and 36 t km^{-2} yr^{-1}; catchment area = 4.53 and 2.24 km^2,
411 respectively) and those observed by Laignel et al. (2006) and Landemaine (2016) in larger catchments
412 in Normandy, France (Austreberthe: 16 t km^{-2} yr^{-1} and Andelle: 21 t km^{-2} yr^{-1}). On the other hand, the
413 SY results for the two years monitoring of the Pommeroye catchment are lower than those measured
414 by Walling et al. (2002) in UK catchments (Belmont, Jubilee, and Lower Smisby; catchment area = 1.5,
415 0.3, and 2.6 km^2, respectively) with a specific sediment yield between 70.6 and 181.1 t km^{-2} yr^{-1}.

416 A strong variability is observed between the two years of monitoring at the Pommeroye
417 catchment with a difference of 40.6 t km^{-2} yr^{-1}. Supplemental years of monitoring on the Pommeroye
418 catchment would be useful to increase the representativeness of the measured sediment yield.
419 Nevertheless, similar observations were made by Walling et al. (2002) for the catchment of Jubilee
420 and New Cliftonthorpe (NC) in UK where the specific sediment yield varied from 81.1 to 181.1 t km^{-2}
421 yr^{-1} over two years of monitoring for the Jubilee, and from 0.6 to 122.4 t km^{-2} yr^{-1} for the NC.
422 Comparable approaches in Belgium have also shown that hydro-sedimentary responses were highly
423 variable between two distinct hydrologic years (Vandaele and Poesen, 1995; Poesen et al., 1996).
424 Walling et al. (2002) also point out that this variability is not only due to the variability of rainfall
425 amount but also to the temporal variability of the rainfall during the year. This is particularly true in
426 the Pommeroye catchment where rainy events were spread out in time during the first year whereas

427 they mainly grouped over a shorter period during the second year. This succession of rainy events
428 during a short time interval may cause a saturation of the infiltration capacity of the soil and the
429 creation of a slaking crust in loess environments (Le Bissonnais et al., 2002).

430 Because of the heterogeneity of the rainfall events, only 6% of the erosive events exported
431 21 t of sediment, i.e. 40% of the sediment flux transported over the two years. Some authors also
432 observed that a few numbers of erosive episodes were responsible for a large part of the exported
433 sediment. Indeed, Nu-Fang et al. (2011) showed that 90% of the hydro-sedimentary flux could be
434 produced by only nine erosive events for a hydrological year in the Wangjiaqiao catchment near the
435 Three Gorges dam in China. Estrany et al. (2009) also observed for the Mediterranean catchment
436 that 90% of the hydro-sedimentary flux was transported during only 0.13% of the time over the
437 studied period. Similar observations were made by Lana-Renault and Regüés, (2009) in Spain where
438 75% of the hydro-sedimentary flux were produced by only 15% of the erosive events over the
439 studied period. These results clearly underline the variability of the hydro-sedimentary production in
440 small agricultural catchments for which most of the hydro-sedimentary fluxes are produced by a
441 small number of events. Strong seasonal variability was identified over the two years of monitoring
442 at the Pommeroye catchment. Most of the hydro-sedimentary transfer was produced in winter (55%)
443 and autumn (42%). Only 3% of the sediment flux is produced during the spring and summer periods
444 although the rainfall intensities are the most important. This can be mainly explained by the state of
445 the soil surface, more particularly by a better crop cover on the agricultural plots which plays an
446 important role of protection against the rainfall impact.

447 The employed statistical analyses showed that SSY and Q_{max} have the best correlation (r^2 =
448 0.91). It is reasonable to expect a high degree of correlation between these two variables considering
449 that runoff is produced by rainfall excess in Hortonian environments, and where Q_{max} is a function of
450 rainfall intensity and duration. It has been noticed in the literature that Q_{max} is a meaningful variable

451 because it exerts influence on both the production and the transfer functions of sediment dynamics
452 (Duvert et al., 2012). Positives correlations between sediment and rainfall variables were also
453 observed (SY vs. R_{time}, and SY vs. R_a), but not as robust as the relationships between SSY and
454 discharge variables. The correlation between the amount of rainfall and the sediment yield shows a
455 threshold at 36 mm for which the erosive events are the most important. Below this threshold, a
456 dispersion of the data cloud is observed, which seems to indicate that other forcing parameters must
457 be considered, such as the surface state of the soils. As emphasized by Evrard et al. (2010), the state
458 of the soil surface result from rainfall conditions and the vegetation growing system in place. In
459 addition, agricultural operations modify the state of the soil surface and are practiced at different
460 times of the year. Depending on the temporal variability of soil surface conditions (soil erodibility,
461 roughness, crop cover) in the catchment, it can be assumed that the erosion processes will show
462 significant spatial and temporal variability throughout the year (Cerdan et al., 2002). To better assess
463 the impact of these parameters on the hydro-sedimentary response, monitoring of the soil surface
464 conditions over time, with an adapted spatio-temporal resolution, could give further valuable
465 information. The consideration of cultural practices and soil quality is therefore a continuation of this
466 work, which is presented in further detail in Patault (2018).

467 Surprisingly, the amount of 48 h-antecedent rainfall is not correlated with the hydro-
468 sedimentary response. Thus, the parameter cannot be considered as an explanatory factor even
469 though this parameter is commonly used in runoff erosion models developed for catchments located
470 on the European loess belt: i.e. *STREAM* and *WATERSED* models (Cerdan et al., 2002; Souchère et al.,
471 2003; Landemaine, 2016). In addition, maximum rainfall intensities are not correlated with the
472 hydro-sedimentary response (expect for the suspended sediment concentration). These results are
473 contradictory with those published by Nu-Fang et al. (2011) and suggest that the modification of
474 farming practices and the farmer's efforts to get an important crop cover over the plots throughout
475 the year allows a reduction in the impact of the rain splash effect. In addition, the rainfall kinetic

476 energy seems to be a more representative parameter of detachment and transport of suspended
477 particulate matter than the rainfall intensity in our study site and shows a reasonably good
478 correlation with the maximum suspended sediment concentration observed at the outlet of the
479 Pommeroye catchment.

480 The correlation between the maximum sediment concentration and the peak flow was found
481 as not statistically significant, indicating that the relationship is more complex between these two
482 variables. As pointed out by Williams (1989), hysteresis effects can be observed during erosive
483 episodes and multiple sediment sources can be mobilized. Sources that cause sediment
484 remobilization may include diffuse erosion on plots or concentrated erosion through ephemeral
485 gullies. In the Pommeroye catchment, the hydro-sedimentary response is complex, and it is difficult
486 to identify the exact sediment sources responsible of the sediment transfer via the flood
487 hydrographs. An alternative approach could be to quantify the contribution of these different
488 sources via the use of a GIS model. These approaches have been successfully used by Cerdan et al.
489 (2002) and Stolte et al. (2003). For example, the *STREAM* model (Cerdan et al., 2001; Souchère et al.,
490 2003) and more recently the *WATERSED* model (Landemaine, 2016) allow the prediction of diffuse
491 and concentrated erosion in catchments. These models considered the catchment morphology, the
492 rainfall characteristics, and the soil surface conditions to quantify the hydro-sedimentary response
493 for a specific rain event and to evaluate the spatial variability of sediment remobilization. We
494 consider this future particularly suitable for the Pommeroye catchment, intending to allow the
495 identification of the spatial variability of the sediment sources during an erosive episode and to
496 quantify their respective contributions.

497 These two years of experimental monitoring are a first step for an on-going erosion reduction
498 project (Patault, 2018) and will be used to calibrate the *WATERSED* erosion model. Moreover, this
499 will allow to evaluate the efficiency of hypothetical erosion control measures (fascines, hedges, grass

strips) on the studied catchment. The observations on the Pommeroye catchment and the *WATERSED* modelling also should allow to upscale to larger areas (Canche catchment) which have the same erosion problems (e.g. Patault et al., 2019) but not the same logistics in terms of monitoring.

6 Conclusion

This study reports on a detailed record of the hydro-sedimentary response to rainfall events in the small agricultural catchment of the Pommeroye in Northern France. The research was based on a high-frequency (6 min) monitoring of rainfall, runoff, and suspended sediment transport over a period of two hydrological years (April 2016 – April 2018), in a challenging context where the studied catchment is a lacking a perennial hydrographic network. A high inter-annual variability of the sediment yield has been observed. Over two years, the specific sediment yield ranges from 29.4 to 70 t km^{-2} yr^{-1} suggesting a large heterogeneity of the erosive events. Most of the sediment was transported in winter (55%) and autumn (42%) whereas it was less significant in summer and spring (3%). At the event scale, the results showed high variability in their hydro-sedimentary response. A small number of events (6%) were responsible for a large proportion of the sediment yield (40%). The multivariate statistical analyses showed that the best correlation is observed between SSY and Q_{max} and that the rainfall variables: R_a and R_{time}, are the most relevant factors controlling the hydro-sedimentary response. Rainfall intensity and rainfall kinetic energy explained the highest values of suspended sediment at the outlet, while the 48 h-antecedent rainfall is not statistically significant with the hydro-sedimentary parameters. These results confirm the high variability of the hydro-sedimentary response to rainfall events, the complexity of the erosion processes in the agricultural plains of North-Western Europe, and improve our understanding of the possible connections or disconnections between the water and the sediment transport pathways. The findings are important for watershed stakeholders, as it enhances our understanding on the spatio-temporal variability of sediment fluxes induce by mudflows and their main controlling factors.

Acknowledgements

This work was financially supported by the Mines-Telecom Institute of Lille-Douai, with additional funding provided by the Water Agency of Arthois-Picardie (QUASPER project). We would also like to acknowledge technical support from the SYMCEA and the regional Chamber of Agriculture Nord-Pas-de-Calais, France. The authors are grateful to M.Desmons, the landowner who permitted instrumentation of the catchment.

References

AFNOR (1986). *NF ISO 4359 – Mesures de débit des liquides dans les canaux découverts – Canaux jaugeurs à col rectangulaire, à col trapézoïdal et à col en U*.

Alexandre, H. (2015). *Quantification de l'efficacité des fascines : diagnostic initial du bassin versant de la Pommeroy et paramétrage d'un modèle de ruissellement/érosion*. 54p.

Bagarello, V., Di Stefano, C., Ferro, V., Pampalone, V. (2017). Predicting maximum annual values of event soil loss by USLE-type models. *Catena*, 155, 10-19. http://dx.doi.org/10.1016/j.catena.2017.03.002

Beckelynck, J. (1981). *Traitement régionalisé des paramètres contribuant à la gestion des nappes: application à la modélisation de la nappe de la craie dans le bassin de l'Aa et de la moyenne Lys*. Université des Sciences et Techniques de Lille. Retrieved from https://ori-nuxeo.univ-lille1.fr/nuxeo/site/esupversions/1ea8eb07-e140-446e-be38-7383cefdb7fc

Brown, L. C., and Foster, G. R. (1987). Storm erosivity using idealized intensity distributions. *Trans. ASAE*, 30, 379-386.

Brandt, C. J. (1989). The size distribution of throughfall drops under vegetation canopies. *Catena*, 16, 507-524. https://doi.org/10.1016/0341-8162(89)90032-5

Capra, A. (1993). Ephemeral gully and gully erosion in cultivated land: a review. *Drainage Basins and Catchment Management*, 109–141.

Castillo, C., & Gomez, J. A. (2016). A century of gully erosion research: Urgency, complexity and study approaches. *Earth-Science Reviews*, *160*, 300–319. https://doi.org/10.1016/j.earscirev.2016.07.009

Cerdan, O., Le Bissonais, Y., Souchère, V., Martin, P., Lecomte, V. (2002). Sediment concentration in interill flow: interactions between soil surface conditions, vegetation and rainfall. *Earth Surface Processes*, *205*(27), 193–205. https://doi.org/10.1002/esp.314

Cerdan, O., Souchère, V., Lecomte, V., Couturier, A., Le Bissonnais, Y. (2001). Incorporating soil surface crusting processes in an expert-based runoff model: Sealing and transfer by runoff and erosion related to agricultural management. *Catena*, *46*(2–3), 189–205. https://doi.org/10.1016/S0341-8162(01)00166-7

559 Cerdan, O., Souchère, V., Lecomte, V., Couturier, A., Le Bissonnais, Y. (2002). Incorporating soil
560 surface crusting processes in an expert-based runoff model: Sealing and transfer by runoff and
561 erosion related to agricultural management. *Catena*, *46*(2–3), 189–205.
562 https://doi.org/10.1016/S0341-8162(01)00166-7

563 Cerdan, O., Govers, G., Le Bissonnais, Y., Van Oost, K., Poesen, J., Saby, N., Gobin, A., Vacca, A.,
564 Quinton, J., Auerswald, K., Klik, A., Kwaad, F. J. P. M., Raclot, D., Ionita, I., Rejman, J., Rousseva,
565 S., Muxart, T., Roxo, M. J., Dostal, T. (2010). Rates and spatial variations of soil erosion in
566 Europe: A study based on erosion plot data. *Geomorphology*, *122*(1–2), 167-177.
567 https://doi.org/10.1016/j.geomorph.2010.06.011

568 Delmas, M., Pak, L. T., Cerdan, O., Souchère, V., Le Bissonnais, Y., Couturier, A., Sorel, L. (2012).
569 Erosion and sediment budget across scale: A case study in a catchment of the European loess
570 belt. *Journal of Hydrology*, *420–421*, 255–263. https://doi.org/10.1016/j.jhydrol.2011.12.008

571 Dufresne, M., Vasquez, J. T., Fischer, M. (2010). Etude hydraulique des venturis à section
572 exponentielle ISMA. Equipe "hydraulique urbaine", ENGEES - IMFS. 29p.

573 Duvert, C., Nord, G., Gratiot, N., Navratil. O., Nadal-Romero, E., Mathys, N., Némery, J., Regues, D.,
574 Garcia-Ruiz, J.M., Gallart, F., Esteves, M. (2012). Towards prediction of suspended sediment
575 yield from peak discharge in small erodible mountainous catchments (0.45 - 22 km²) of France,
576 Mexico and Spain. *Journal of Hydrology*, *454-455*, 42-55.
577 http://dx.doi.org/10.1016/j.jhydrol.2012.05.048

578 Estrany, J., Garcia, C., & Batalla, R. J. (2009). Suspended sediment transport in a small Mediterranean
579 agricultural catchment. *Earth Surface Processes and Landforms*, *34*(March), 155–161.
580 https://doi.org/10.1002/esp

581 Evrard, O., Bielders, C. L., Vandaele, K., Van Wesemael, B. (2007). Spatial and temporal variation of
582 muddy floods in central Belgium, off-site impacts and potential control measures. *Catena*,
583 *70*(3), 443–454. https://doi.org/10.1016/j.catena.2006.11.011

584 Evrard, O., Nord, G., Cerdan, O., Souchère, V., Le Bissonnais, Y., Bonté, P. (2010). Modelling the
585 impact of land use change and rainfall seasonality on sediment export from an agricultural
586 catchment of the northwestern European loess belt. *Agriculture, Ecosystems and Environment*,
587 *138*(1–2), 83–94. https://doi.org/10.1016/j.agee.2010.04.003

588 Foster, G. R. (1986). Understanding ephemeral gully erosion. In *Soil Conservation vol 2* (Vol. 2, pp.
589 90–125).

590 Foucher, A. (2015). Reconstruction de la cascade sédimentaire en contexte de plaine agricole
591 drainée: Sources, voies de transfert et stockage de matière dans le bassin versant du Louroux
592 (Indre-et-Loire). Ph.D. Thesis. Université François-Rabelais, Tours, France. 203p.

593 Foucher, A., Salvador-Blanes, S., Evrard, O., Simonneau, A., Chapron, E., Courp, T., Cerdan, O.,
594 Lefévre, I., Adriaensen, H., Lecompte, F., Desmet, M. (2015). Increase in soil erosion after
595 agricutlural intensification: Evidence from a lowland basin in France. *Anthropocene*, *7*, 30-41.
596 https://doi.org/10.1016/j.ancene.2015.02.001

597 Frankl, A., Nyssen, J., De Dapper, M., Haile, M., Billi, P., Munro, R. N., Poesen, J. (2011). Linking long-
598 term gully and river channel dynamics to environmental change using repeat photography
599 (Northern Ethiopia). *Geomorphology*, *129*(3–4), 238–251.

https://doi.org/10.1016/j.geomorph.2011.02.018

Gay, A., Cerdan, O., Delmas, M., Desmet, M. (2014). Variability of suspended sediment yields within the Loire river basin (France). *journal of Hydrology*, *519*, 1225-1237. https://doi.org/10.1016/j.jhydrol.2014.08.045

Gay, A., Cerdan, O., Mardhel, V., Desmet, M. (2016). Application of an index of sediment connectivity in a lowland area. *J Soils Sediments*, *16(1)*, 280-293. https://doi.org/10.1007/s1136

Giménez, R., Casalí, J., Grande, I., Díez, J., Campo, M. a., Álvarez-Mozos, J., Goñi, M. (2012). Factors controlling sediment export in a small agricultural watershed in Navarre (Spain). *Agricultural Water Management*, *110*, 1–8. https://doi.org/10.1016/j.agwat.2012.03.007

Grangeon, T., Manière, L., Foucher, A., Vandromme, R., Cerdan, O., Evrard, O., Pene-Galland, I., Salvador-Blanes, S. (2017). Hydro-sedimentary Dynamics of a Drained Agricultural Headwater Catchment: A Nested Monitoring Approach. *Vadose Zone J.*, *16(12).* https://doi.org/10.2136/vzj2017.05.0113

Goodwin, N. R., Armston, J. D., Muir, J., Stiller, I. (2017). Monitoring gully change: A comparison of airborne and terrestrial laser scanning using a case study from Aratula, Queensland. *Geomorphology*, *282*, 195–208. https://doi.org/10.1016/j.geomorph.2017.01.001

Heckmann, T., Cavalli, M., Cerdan, O., Foerster, S., Javaux, M., Lode, E., Smetanova A., Vericat, D., Brardinoni, F. (2018). Indices of sediment connectivity: opportunities, challenges and limitations. *Earth-Science Reviews*. https://doi.org/10.1016/j.earscirev.2018.08.004

Laignel, B., Dupuis, E., Durand, A., Dupont, J. P., Hauchard, E., Massei, N. (2006). Erosion balance in the watersheds of the western Paris Basin by high-frequency monitoring of discharge and suspended sediment in surface water. *Comptes Rendus - Geoscience*, *338*(8), 556–564. https://doi.org/10.1016/j.crte.2006.03.010

Lana-Renault, N., & Regüés, D. (2009). Seasonal patterns of suspended sediment transport in an abandoned farmland catchment in the Central Spanish Pyrenees. *Earth Surface Processes and Landforms*, *34*(June), 155–161. https://doi.org/10.1002/esp

Landemaine, V., Gay, A., Cerdan, O., Salvador-Blanes, S. Rodrigues, S. (2015). Morphological evolution of a rural headwater stream after channelisation. *Geomorphology*, *230*, 125-137. https://doi.org/10.1016/j.geomorph.2014.11.011

Landemaine, V. (2016). *Érosion des sols et transferts sédimentaires sur les bassins versants de l'Ouest du Bassin de Paris : analyse, quantification et modélisation à l'échelle pluriannuelle*. Université de Rouen Normandie. 235p.

Le Bissonnais, Y., Thorette, J., Bardet, C., Daroussin, J. (2002). *L'Erosion Hydrique Des Sols En France*. Retrieved from http://prodinra.inra.fr/?locale=fr#!ConsultNotice:69099

Lefrançois, J. (2007). Dynamiques et origines des matières en suspension sur de petits bassins versants agricoles sur schiste., 280.

Li, Z., Zhang, Y., Zhu, Q., Yang, S., Li, H., Ma, H. (2017). A gully erosion assessment model for the Chinese Loess Plateau based on changes in gully length and area. *Catena*, *148*, 195–203. https://doi.org/10.1016/j.catena.2016.04.018

639 Marzolff, I., Ries, J. B., & Poesen, J. (2011). Short-term versus medium-term monitoring for detecting
640 gully-erosion variability in a Mediterranean environment. *Earth Surface Processes and*
641 *Landforms*, *36*(12), 1604–1623. https://doi.org/10.1002/esp.2172

642 Morgan, R. P. C., and Duzant, J. H. (2008). Modified MMF (Morgan-Morgan-Finney) model for
643 evaluating effects of crops and vegetation cover on soil erosion. *Earth Surface Processes and*
644 *Landforms*, *33*, 90-106. https://doi.org/10.1002/esp.1530

645 Nachtergaele, J., & Poesen, J. (1999). Assessment of soil losses by ephemeral gully erosion using high-
646 altitude (stereo) aerial photographs. *Earth Surface Processes and Landforms*, *24*(8), 693–706.
647 https://doi.org/10.1002/(SICI)1096-9837(199908)24:8<693::AID-ESP992>3.0.CO;2-7

648 Nachtergaele, J., Poesen, J., & Govers, G. (2002). Ephemeral gullies a spatial and temporal analysis of
649 their characteristics, importance and prediction. *Eeen Ruimtelijke En Temporele Analyse van de*
650 *Karakteristieken, Het Belang En de Voorspelling van Tijdelijke Ravijnen*, (2), 159–182.
651 https://doi.org/10.4000/belgeo.16167

652 Nadal-Romero, E., Regüés, D., & Latron, J. (2008). Relationships among rainfall, runoff, and
653 suspended sediment in a small catchment with badlands. *Catena*, *74*(2), 127–136.
654 https://doi.org/10.1016/j.catena.2008.03.014

655 Nu-Fang, F., Zhi-Hua, S., Lu, L., Cheng, J. (2011). Rainfall, runoff, and suspended sediment delivery
656 relationships in a small agricultural watershed of the Three Gorges area, China. *Geomorphology*,
657 *135*(1–2), 158–166. https://doi.org/10.1016/j.geomorph.2011.08.013

658 Patault, E. (2018). *Analyse multi-échelle des processus d'érosion hydrique et de transferts*
659 *sédimentaires en territoire agricole: exemple du bassin versant de la Canche*. Ph.D Thesis. IMT
660 Lille Douai, France. 300p.

661 Pataut, E., Alary, C., Franke, C., Abriak, N-E. (2019). Quantification of tributaries contributions using a
662 confluence-based sediment fingerprinting approach in the Canche river watershed (France).
663 *Science of the Total Environment*, *688*, 457–469.
664 https://doi.org/10.1016/j.scitotenv.2019.02.458

665 Panagos, P., Meusburger, K., Ballabio, C., Borrelli, P., Alewell C. (2014). Soil erodibility in Europe: A
666 high-resolution dataset based on LUCAS. S*cience of the Total Environment, 479-480*, 189-200.
667 http://dx.doi.org/10.1016/j.scitotenv.2014.02.010

668 Panagos, P., Ballabio, C., Borrelli, P., Meusburger, K., Klik, A., Rousseva, S., Tadic, M. P., Michaelides,
669 S., Hrabalikova, M., Olsen, P., Aalto, J., Lakatos, M., Rymszewicz, A., Dumitrescu, A., Begueria, S.,
670 Alewell, C. (2015b). Rainfall erosivity in Europe. *Science of the Total Environment, 511*, 801-814.
671 https://doi.org/10.1016/j.scitotenv.2015.01.008

672 Poesen, J. (1993). Gully typology and gully control measures in the European loess belt. *Farm Land*
673 *Erosion: In Temperate Plains Environment and Hills*, 221–239. https://doi.org/10.1016/B978-0-
674 444-81466-1.50024-1

675 Poesen, J. W., Vandaele, K., & Wesemael, B. V. a. N. (1996). Contribution of gully erosion to sediment
676 production on cultivated lands and rangelands. *Erosion and Sediment Yield: Global and Regional*
677 *Perspectives (Proceedings of the Exeter Symposium July 1996). IAHS Publ.*, *236*(236), 251–266.

678 Poesen, J. (2018). Soil erosion in the Anthropocene: Research needs. *Earth Surfaces Processes and*
679 *Landforms*, 43, 64-84. https://doi.org/10.1002/esp.4250

680 Sherriff, S. C., Rowan, J. S., Melland, A. R., Jordan, P., Fenton, O., O hUallachain, D. (2015).
681 Investigating suspended sediment dynamics in contrasting agricultural catchments using ex situ
682 turbidity-based suspended sediment monitoring. *Hydrol. Earth Syst. Sci.*, *19*, 3349-3363.
683 https://doi.org/10.5194/hess-19-3349-2015

684 Souchère, V., Cerdan, O., Ludwig, B., Le Bissonnais, Y., Couturier, A., Papy, F. (2003). Modelling
685 ephemeral gully erosion in small cultivated catchments. *Catena*, *50*(2–4), 489–505.
686 https://doi.org/10.1016/S0341-8162(02)00124-8

687 Stolte, J., Liu, B., Ritsema, C. J., Van Den Elsen, H. G. M., Hessel, R. (2003). Modelling water flow and
688 sediment processes in a small gully system on the Loess Plateau in China. *Catena*, *54*(1–2), 117–
689 130. https://doi.org/10.1016/S0341-8162(03)00060-2

690 Thompson, D. B. (2006). The Rational Method. *Civil Engineering Departement Texas Tech University*.
691 7p. Available at: http://drdbthompson.net/writings/rational.pdf

692 Valcárcel, M., Taboada, M. T., Paz, A., Dafonte, J. (2003). Ephemeral gully erosion in northwestern
693 Spain. *Catena*, *50*(2–4), 199–216. https://doi.org/10.1016/S0341-8162(02)00139-X

694 Valentin, C., Poesen, J., & Li, Y. (2005). Gully erosion: Impacts, factors and control. *Catena*, *63*(2–3),
695 132–153. https://doi.org/10.1016/j.catena.2005.06.001

696 Vandaele, K., & Poesen, J. (1995). Spatial and temporal patterns of soil erosion rates in an agricultural
697 catchment, central Belgium. *Catena*, *25*(95), 213–226. https://doi.org/10.1016/0341-
698 8162(95)00011-G

699 Vanmaercke, M., Poesen, J., Verstraeten, G. de Vente, J., Ocakoglu, F. (2011). Sediment yield in
700 Europe: Spatial patterns and scale dependency. *Geomorphology*, *130*(3-4), 142-161.
701 https://doi.org/10.1016/j.geomorph.2011.03.010

702 Verstraeten, G., & Poesen, J. (2001). Factors controlling sediment yield from small intensively
703 cultivated catchments in a temperate humid climate. *Geomorphology*, *40*, 123-144.
704 https://doi.org/10.1016/s0169-555x(01)00040-x

705 Walling, D. E., Russell, M. A., Hodgkinson, R. A., Zhang, Y. (2002). Establishing sediment budgets for
706 two small lowland agricultural catchments in the UK. *Catena*, *47*(4), 323–353.
707 https://doi.org/10.1016/S0341-8162(01)00187-4

708 Williams, G. P. (1989). Sediment concentration versus water discharge during single hydrologic
709 events in rivers. *Journal of Hydrology*, *111*(1–4), 89–106. https://doi.org/10.1016/0022-
710 1694(89)90254-0

711 Wischemeir, W., and Smith, D. (1978). Predicting rainfall erosion losses: a guide to conservation
712 planning. *Agricultural handbook*, No. 537, U.S. Departement of Agriculture, Washington DC,
713 USA.

714

715